The Third International Bridge Seismic Workshop, 3rd IBSW
Seattle, Washington, USA - October 1st to 4th, 2019

CAPACITY-BASED INELASTIC DISPLACEMENT SPECTRA FOR REINFORCED CONCRETE BRIDGE COLUMNS SUBJECTED TO FAR-FIELD AND NEAR-FAULT GROUND MOTIONS

K. C. Chang[(1)], P. H. Wang[(2)], W. C. Cheng[(3)]

[(1)] Professor, Department of Civil Engineering, National Taiwan University, Taipei, Taiwan, ciekuo@ntu.edu.tw
[(2)] Assistant Technologist, National Center for Research on Earthquake Engineering, Taipei, Taiwan, phwang@ncree.narl.org.tw
[(3)] Graduate Student, Department of Civil Engineering, National Taiwan University, Taipei, Taiwan, s971337@gmail.com

Abstract

Capacity-based inelastic displacement spectra that comprise an inelastic displacement ratio (C_R) spectrum and the corresponding damage index (DI) spectrum are proposed in this study to aid seismic design and evaluation of reinforced concrete (RC) bridges. Nonlinear time history analyses of SDOF systems are conducted using a versatile smooth hysteretic model when subjected to far-field and near-fault ground motions. It is demonstrated that the Park and Ang's damage index can be a good indicator for assessing the actual visible damage condition of column regardless of its loading history, providing a better insight into the seismic performance of bridges. The computed spectra for near-fault ground motions show that as the magnitude of pulse period ranges increases from NF1 (0.5 - 2.5 s) to NF2 (2.5 - 5.5 s), the spectral ordinates of the C_R and DI spectra increase moderately. In contrast, the computed spectra do not show much difference between NF2 and NF3 (5.5 - 10.5 s) when the period of vibration $T_n \leq 1.5$ s, after which the spectral ordinates of NF3 tend to increase obviously whereas those of NF2 decrease with increasing T_n. Moreover, when relative strength ratio R = 5.0, nearly all of the practical design scenarios could not survive NF3. Based on the computed spectra, C_R and DI formulae are presented as a function of T_n, R, and various design parameters for far-field and near-fault ground motions. Finally, application of the proposed spectra to the performance-based seismic design of RC bridges is presented using DI as the performance objective, and an example bridge will be used to demonstrate the applicability of the proposed spectra.

Keywords: Reinforced concrete; bridge columns; inelastic displacement; damage index; near-fault

1. Introduction

To aid seismic evaluation of new designed or existing bridges, various analysis methods are available according to the seismicity, regularity, complexity, and importance of bridges. It can be found that current seismic design and evaluation of bridges (e.g., the seismic retrofitting manual for highway structures, FHWA, 2006; the AASHTO guide specification for seismic bridge design, 2011; the Caltrans Seismic Design Criteria, SDC, 2013; the Eurocode 8 on design of structures for earthquake resistance part 2: bridges, 2005) tends towards the well-known displacement coefficient method (FEMA 273, 1997). The key element of the displacement coefficient method is the displacement coefficient (or referred to as inelastic displacement ratio, hereafter) that allows maximum inelastic displacement of a system to be estimated from its maximum elastic displacement. Many researchers have focused on this area based on statistical study on nonlinear time history analyses of SDOF systems subjected to a suite of earthquake ground motions. Instead of the direct method mentioned above, inelastic displacement ratio can also be derived from existing R_μ-μ-T_n relations, where R_μ is the strength reduction factor due to ductility μ. In particular, Fajfar (1999) utilized the R_μ formula proposed by Vidic et al. (1994) to derive the inelastic displacement ratio, on which the coefficient C_1 in FEMA 273 (1997) and also the R_d factor of FHWA (2006) were based.

Most, if not all, of the inelastic displacement ratios mentioned above are based on polygonal hysteretic models, such as the elastoplastic (EPP) model, the bilinear model, and stiffness and/or strength degrading models. Nevertheless, real hysteresis behaviors of structures are smooth rather than piecewise linear with abrupt stiffness changes. Furthermore, the severity and characteristics of degradation of hysteresis behaviors depend mainly on the structural system and the design parameters of its components, thus affecting the resulting seismic responses and damage state. But apparently current published formulae for the inelastic displacement ratio lack this kind of link. For bridge applications, there should be a better chance to fill this gap than for building applications since the seismic response of a bridge is relatively simple and primarily dominated by its substructure (i.e., bridge pier or column). The authors recently proposed a versatile smooth hysteretic model (SHM; Wang et al. 2017) that can realistically simulate the seismic behaviors of reinforced concrete bridge columns with the effects of various design parameters. Most importantly, it was demonstrated that the damage index proposed by Park and Ang (1985) can be used to accurately predict the onset of strength deterioration. Furthermore, it was found in this research that the damage index can be a good indicator for assessing the actual visible damage conditions of column regardless of its loading history. Therefore, seismic analysis via this model can obtain not only the maximum responses of a column but also its damage condition under a given ground motion, providing a better insight into its seismic performance.

The objective of this paper is to statistically compute the inelastic displacement ratio and the corresponding damage index (i.e., the so-called capacity-based inelastic displacement spectra) of a SDOF system using the proposed smooth hysteretic model with the effects of various design parameters of RC bridge columns when subjected to both far-field and near-fault ground motions. New formulae for the capacity-based spectra as a function of period of vibration, relative strength ratio, and various design parameters of columns are presented for far-field and near-fault ground motions. Finally, application of the proposed spectra to the performance-based seismic design of bridges is presented using the damage index as the performance objective, and an example bridge will be used to demonstrate the applicability of the proposed spectra.

2. Smooth hysteresis model

The smooth hysteretic model (SHM) used to perform the nonlinear time history analysis of SDOF system is proposed by Wang et al. (2017). The model is based on the Bouc-Wen model (1976) with significant modification to consider hysteretic rules for damage accumulation and path dependence of RC bridge columns. The relationship between the restoring force and displacement of system is described by a differential equation as follows.

$$\dot{z(t)} = h(z)\frac{\{A\dot{u}-\nu[\beta|\dot{u}||z|^{n-1}z+\gamma\dot{u}|z|^n]\}}{\eta} \quad (1)$$

$$h(z) = 1 - \xi_1 \exp\left\{-\frac{[z\ sgn(\dot{u}) - q\ z_u]^2}{\xi_2^2}\right\}\left|\frac{sgn(\dot{u}) + sgn(z)}{2}\right| \quad (2)$$

where z and u are the normalized restoring force and displacement of system, respectively; A, β, γ, and n are parameters that determine the basic shape of the z-u relation; ν and η are the strength and stiffness degradation parameters, respectively; $h(z)$ is the pinching function in which ξ_1 controls the severity of pinching, ξ_2 controls the spread of pinching, and q defines the force level z at which pinching reaches its maximum effect; $sgn()$ is the signum function; and z_u is the ultimate value of z.

To consider strength deterioration, the model utilizes the damage index (DI as defined in Eq. 3) proposed by Park and Ang (1985) to initiate strength deterioration until DI is accumulated to a threshold value DI_o.

$$DI = \frac{\delta_m}{\delta_u} + \lambda \frac{\int dE}{F_y \delta_u} \quad (3)$$

where δ_m is the maximum displacement of column; δ_u is the ultimate displacement capacity of column under monotonic loading; $\int dE$ is the accumulated hysteretic energy dissipation; F_y is the yield force; and λ is a parameter to correlate hysteretic energy dissipation to damage, which can be calculated by setting DI equal to one at the ultimate state of column when the strength of column drops to 80% of its peak value.

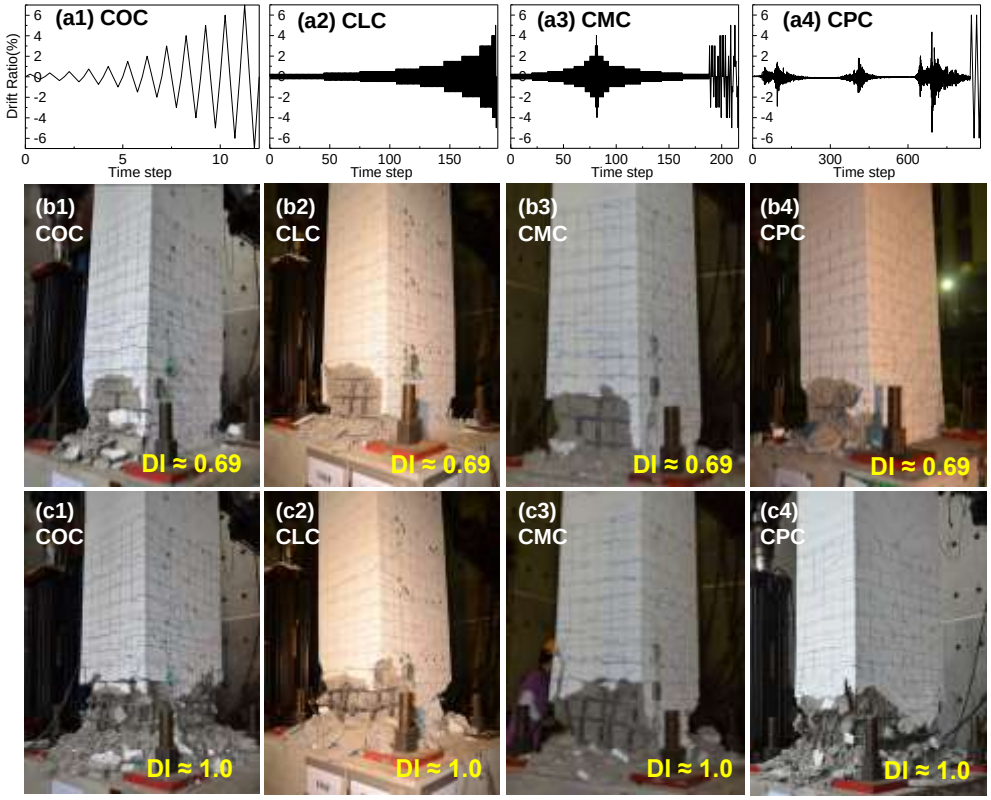

Fig. 1 – Correlation between damage index and actual damage condition

It was proved in Wang et al. (2017) that the damage index can accurately predict the onset of strength deterioration regardless of the loading history a column was subject to. Furthermore, it was found in this research (Figure 1) that the damage index can also be correlated well with the actual damage conditions of column. In the figure, four column specimens having identical design parameters were subjected to very different loading histories. Specimens COC and CLC underwent monotonically increasing cyclic loadings with one cycle and many cycles at each drift level, respectively, while Specimen CMC suffered monotonically increasing cyclic loading which was accompanied with monotonically decreasing as well as irregular cyclic loadings. In Specimen CPC, pseudo-dynamic loading test was conducted using three consecutive ground

motion records with long duration characteristics, which was followed by extra cyclic loading test using two cycles of 6% drift ratio to exhaust the column. Figures 1(b1) to 1(b4) show the damage conditions of the four columns when their damage indices were accumulated to around 0.69 (DI_o) corresponding to the onset of strength deterioration. The four columns show similar damage states with spalling of cover concrete and slight buckling of longitudinal reinforcements. Figures 1(c1) to 1(c4) further show the damage conditions of the four columns at DI close to 1.0 that corresponds to 20% strength loss. Again, similar damage conditions can be seen in the four columns with significant crushing of confined concrete, severe buckling of longitudinal reinforcements, and severe loosening of transverse reinforcements at 135 and 90 degree hooks. Therefore, the DI can be a good indicator for assessing the actual damage conditions of column regardless of its loading history, which provides a bridge between analytical reuslt and actual visible damage.

3. Model identification for RC bridge columns with various design parameters

In order to consider the effects of design parameters of RC bridge columns on deteriorated hysteresis behaviors and thus on the computed capacity-based inelastic displacement spectra, model identifications from relevant experimental data are presented first in this section. The design parameters of RC bridge columns considered include the longitudinal and transverse reinforcement ratios, the aspect ratio, and the axial load ratio. Experimental data focusing on these effects are mainly obtained from the structural performance database of Pacific Earthquake Engineering Research Center (PEER 2003). Table 1 lists the main design parameters of the tested RC column specimens used in this research. Specimens 407 and 430 (Leman and Moehle, 2000) having different amount of longitudinal reinforcements, namely 0.75% and 3.0% of gross cross-sectional area (A_g), respectively, but identical remaining design parameters are used to investigate the effects of column longitudinal reinforcement. Specimens COC/CLC (Wang et al., 2017) and CTR1 (Ou et al., 2015) are used to examine the effects of column transverse reinforcement, while Specimens 415 and 1015 (Leman and Moehle, 2000) for the column aspect ratio. Specimens B1 and B2 (Wehbe et al. 2001) are used to study the effects of column axial load. For each of the column specimens, the model parameters capable of representing specific degradation characteristic were identified using the methodology proposed by Wang et al. (2017), allowing the effects of certain design parameter to be quantitatively evaluated. More detailed discussions can be found in Wang (2017).

Table 1 – Design parameters of columns

Hysteretic Model	M1 (EPP)	M2 (SHM)	M3 (SHM)	M4 (SHM)	M5 (SHM)	M6 (SHM)	M7 (SHM)	M8 (SHM)	M9 (SHM)
Specimen Name	-	1015	415	407	430	COC/CLC	CTR1	B1	B2
Longitudinal Reinforcement Ratio (%)	-	1.5	1.5	0.75	3.0	2.1	2.1	2.2	2.2
Transverse Reinforcement Ratio (%)	-	0.72	0.72	0.72	0.72	1.26	1.79	0.94	0.94
Aspect Ratio	-	10	4.0	4.0	4.0	3.2	3.5	3.8	3.8
Axial Load Ratio ($f_c'A_g$)	-	0.07	0.07	0.07	0.07	0.10	0.10	0.09	0.23
Note: 1. Concrete compressive strength f_c' ranges from 28.1 to 47.3 MPa 2. Yield strength of longitudinal reinforcing steel f_{yl} ranges from 448.7 to 606.8 MPa 3. Yield strength of transverse reinforcing steel f_{yt} ranges from 441.5 to 581.2 MPa									

4. Capacity-based inelastic displacement spectra

The studies on the inelastic displacement ratio mentioned in the introduction are mainly based on seismic responses to far-field ground motions. In contrast, issues regarding the effect of near-fault ground motions, which is characterized by rupture forward directivity towards the site with pronounced velocity pulses (T_p), have received increasing attention since the last decade. However, it is still difficult to well characterize the near-fault directivity effects on seismic responses by a particular featuring period. This study suggests not normalizing the period of vibration T_n by any featuring period but including a wide range of T_p content when

selecting the pulse-like near-fault records for statistical analysis. And similar to the work done by Tothong and Cornell (2007), the near-fault records are categorized into three T_p ranges based on the magnitude of T_p. This allows users to choose one of the three T_p ranges which is most likely to occur at a given bridge site to appropriately represent the site characteristics. In addition, the calculated seismic responses to the three different T_p ranges of near-fault records can also be used to investigate the effects of the magnitude of pulse period.

4.1 Spectrum parameters

The proposed capacity-based inelastic displacement spectra are comprised of an inelastic displacement ratio spectrum and the corresponding damage index spectrum, forming a twin spectrum to provide estimates not only for the displacement demand but also for the damage state of a system under earthquakes. This study focuses on the constant strength inelastic displacement ratio which is defined as

$$C_R = \frac{\Delta_{inelastic}}{\Delta_{elastic}} \tag{4}$$

where $\Delta_{inelastic}$ is the maximum inelastic displacement of a SDOF system with a 5% viscous damping ratio and a lateral yield strength F_y while $\Delta_{elastic}$ is the maximum elastic displacement of the corresponding elastic system having the same T_n and subjected to the same earthquake ground motion.

It should be mentioned that the subscript of C_R is intended to represent that the ratio is based on systems with a constant lateral strength (in contrast to constant ductility, C_μ) as suggested by Miranda (2001). The lateral strength of the system is described by a relative strength ratio R (or strength reduction factor), which is defined as

$$R = \frac{mS_a}{F_y} \tag{5}$$

where m is the mass of the system, and S_a is the elastic spectral acceleration.

The inelastic displacement ratios (C_R) and the corresponding damage indices (DI) as defined in Eq. (3) were computed for SDOF systems having a set of 20 periods of vibration (T_n ranging from 0.05 s to 3.0 s), 9 hysteretic models (M1 to M9) as listed in Table 1, and 5 levels of relative strength ratio (R =1.5, 2, 3, 4, 5) when subjected to 30 far-field (denoted as FF) and 45 pulse-like near-fault (denoted as NF) ground motions.

4.2 Ground motion records

A total of 75 ground motion records including 30 far-field and 45 near-fault ground motions were selected from the ground motion database of Pacific Earthquake Engineering Research Center (PEER, 2013). The far-field records were further classified based on the site class. Two site classes, namely site classes C (denoted as FFC) and D (denoted as FFD) in accordance with the NEHRP classification (2004), were studied in this research. Each of the two site classes contain 15 ground motion records as suggested by Sinković et al. (2018) for the least number used in statistically seismic analysis. The far-field records resulted from 10 different earthquake events with moment magnitude (Mw) ranging from 6.0 to 7.6. On the other hand, the near-fault records with the pulse-like characteristics were classified into three T_p ranges based on the magnitude of T_p. The three T_p ranges, denoted as NF1, NF2, and NF3, have period ranges of 0.5 s - 2.5 s (i.e., including 0.5 s but excluding 2.5 s), 2.5 s - 5.5 s, and 5,5 s - 10.5 s, respectively. The pulse period T_p of each near-fault record was extracted by Baker (2007) using wavelet analysis. It was found in this study that further refinement of the T_p range for NF3 did not show much influences on the calculated seismic responses, and hence the distribution of T_p of NF3 was given wider than those of NF1 and NF2. Besides, it should be noticed that no distinction of near-fault records with different site classes was considered, since the T_p was expected to be the most important characteristic of this kind of ground motions (Iervolino et al. 2012; Ruiz-Garcia 2011). The near-fault records were obtained from 13 different earthquake events with Mw ranging from 5.7 to 7.6, and recorded on site classes B to D. Fig. 2 shows the mean elastic 5% damped spectra for the selected ground motion records, where

the corner periods of the far-field records are approximately consistent with those suggested by FEMA 440 (2005) (i.e., T_c = 0.55 s for site class C and T_c = 0.60 s for site class D).

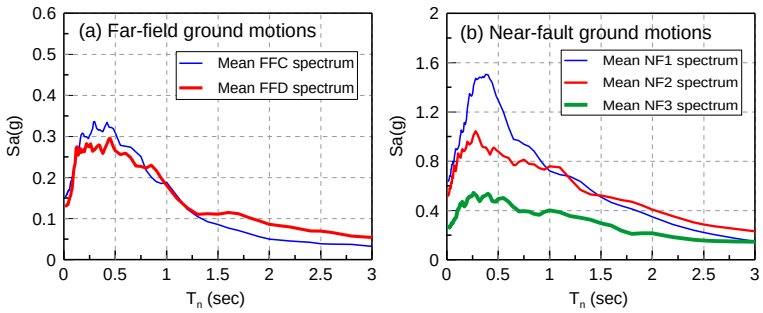

Fig. 2 – Mean elastic 5% damped spectra for (a) far-field ground motions; (b) near-fault ground motions

4.3 Failure criteria

The smooth hysteretic model used in this research may exhibit severe strength deterioration accompanied with significant inelastic displacement demand under earthquake excitation especially when the system has a low lateral strength (a large R) and/or is subjected to pulse-like near-fault ground motions. Therefore, there is a need to define failure criteria both for performing each analysis case and for constructing the capacity-based inelastic displacement spectra. By definition of the hysteresis model, the damage index is calibrated based on DI= 1.0, which corresponds to the lateral strength of column dropping to 80% of its peak value. After this point, the analyzed seismic responses would become unreliable. Besides, in accordance with the experimental observation from columns subjected to different types of cyclic loadings and pseudo dynamic loading, the damage index DI=1.0 also corresponds to severe damage conditions as shown in Figure 1, after which fracture of longitudinal reinforcements associated with abrupt strength drop would occur subsequently. Accordingly, for every analysis case, a column will be deemed failed or collapsed if its damage index DI accumulated at the end of ground excitation is larger than one (or the analysis cannot be continued due to collapse).

On the other hand, in constructing the capacity-based inelastic displacement spectra the mean values of computed inelastic displacement ratios and corresponding damage indices for 15 (far-field or near-fault) ground motions need to be calculated for each suite of spectrum parameters (i.e., a combination of period of vibration T_n, relative strength ratio R, and hysteretic model M). However, as just mentioned, one or more than one of the analyzed cases for 15 (far-field or near-fault) ground motions may show failure at certain spectrum parameters. And inclusion of the collapsed cases in calculating the mean spectra could be meaningless because the analytical results of the collapsed cases are unreliable and even do not help for precautions against collapse. This is far different from the cases commonly seen in the literatures where most of the analytical models were assumed indestructible with the purpose of evaluating the structural demand only. An alternative of the mean spectrum is the median spectrum. However, it was found that the spectral ordinate of the median spectrum is in general less than that of the mean spectrum, and the median DI= 1.0 corresponds to the probability of failure to be around 50% under 15 (far-field or near-fault) ground motions, which tends to the unconservative side in seismic analysis. Therefore, this study proposed to compute the mean spectra based on the non-collapsed cases under 15 (far-field or near-fault) ground motions. Moreover, it was stipulated that if the probability of failure is larger than 20%, a column devised using that suite of spectrum parameters will be deemed unable to survive the considered earthquakes while there will be no corresponding spectral ordinate. Nevertheless, the definition of failure criteria for the proposed capacity-based spectra remains open to discuss in the earthquake engineering community.

4.4 Calculated mean C_R and corresponding DI spectra

Mean C_R and the corresponding DI spectra for 30 far-field and 45 near-fault ground motions were computed by using 9 different hysteretic models (including one EPP model and 8 SHMs) to investigate the effects of ground excitation, column design parameter, and model type on the spectral ordinates. Only selected results

are presented in this paper. Among the 8 SHMs for various design parameters of columns, the M6 model is considered representative of commonly used design scenario of bridges in practice and is used to demonstrate the analyzed results. Besides, the M1 (EPP) model is introduced for comparing the results from polygonal and smooth hysteretic models given that it is widely used in the literatures.

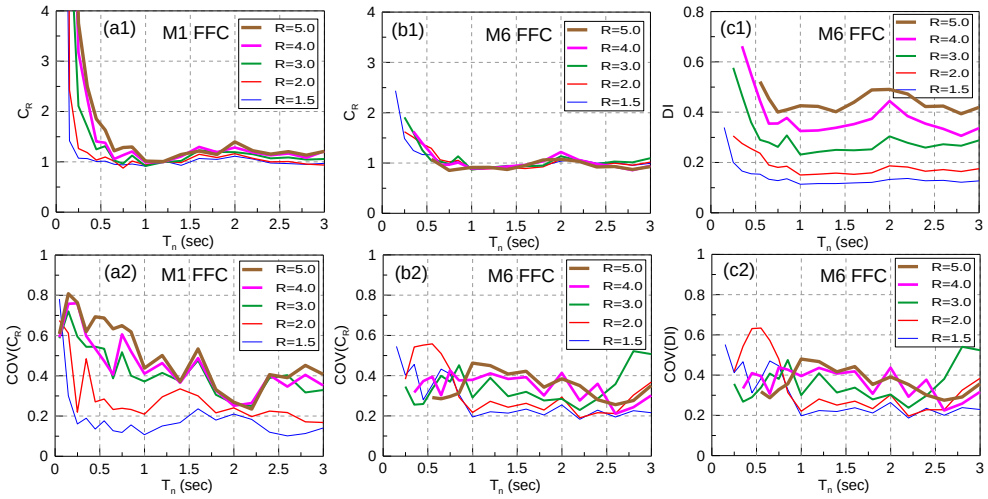

Fig. 3 – Mean C_R and corresponding DI spectra for M6 (SHM) model and mean C_R spectrum for M1 (EPP) model subjected to far-field ground motions recorded on site class C (FFC)

Figure 3 shows the computed mean C_R and the corresponding DI spectra for the M6 model together with the mean C_R spectrum for the M1 model subjected to far-field ground motions recorded on site class C (FFC). It can be obviously seen that in comparison with the conventional C_R spectrum (Fig. 3a1), the proposed spectra (Figs. 3b1 and 3c1) can provide not only the C_R estimate but also its corresponding damage index (DI). In particular, each spectral curve associated with a given relative strength ratio R possesses a period limit. If the period of vibration is shorter than this limit there will be no spectral ordinate or no result. In other words, for a given relative strength ratio R a system with period of vibration shorter than this period limit would fail or collapse under the considered earthquakes. Furthermore, the period limit increases as the relative strength ratio increases. Figure 3(b1) also indicates that the equal displacement rule approximately holds true for period of vibration larger than about 0.7 s regardless of various R values while for short period range (T_n < 0.7 s) the C_R is evidently larger than one and nearly independent of R when $R \geq 2.0$. Besides, the corresponding DI increases with increasing R for all period range of spectrum (Fig. 3c1). On the other hand, the mean C_R spectrum calculated using M1 (EPP) model basically follows the same trend as those conducted by Ruiz-Garcia and Miranda (2003) and FEMA 440 (2005) where C_R always increases as R increases even for long period region (Fig. 3a1). Also given in Figure 3 are the coefficient of variations (COVs) corresponding to the mean values of C_R and DI to show the level of dispersion, which is defined as the ratio of the standard deviation to the mean. In general, the dispersions in C_R for the M1 model are more susceptible to T_n and R as compared to those for the M6 model. Besides, the calculated C_R and DI spectra of M6 model under FFD exhibit increased spectral ordinates when compared to those of M6 model under FFC. This indicates that for FFD, the equal displacement rule is not a conservative measure for long period structures.

Figure 4 shows the mean C_R and corresponding DI spectra for M6 model when subjected to near-fault ground motions with three pulse period T_p ranges. It can be observed that as the magnitude of T_p ranges increases from NF1 (T_p = 0.5 - 2.5 s) to NF2 (T_p = 2.5 - 5.5 s), the spectral ordinates of the C_R and DI spectra increase moderately in the whole spectral region. In contrast, the C_R and DI spectra do not show much difference between NF2 and NF3 (T_p = 5.5 - 10.5 s) when around T_n < 1.5 s, after which the spectral ordinates of NF3 tend to increase obviously whereas those of NF2 decrease with increasing T_n. This reveals that the near-fault ground motions with T_p = 5.5 - 10.5 s would lead to increased seismic responses and damages in long period region. Moreover, for R = 5.0, nearly all of the practical design scenarios considered in this

research could not survive NF3, while some of them (such as the M5, M6, M8 and M9 models) could not even survive when R = 4.0. Figures 4(a3) to 4(c3) indicate that the dispersion levels of the C_R spectra under near-fault ground motions are similar to those under far-field ground motions. More details of the analytical results can be found in Wang et al. (2019).

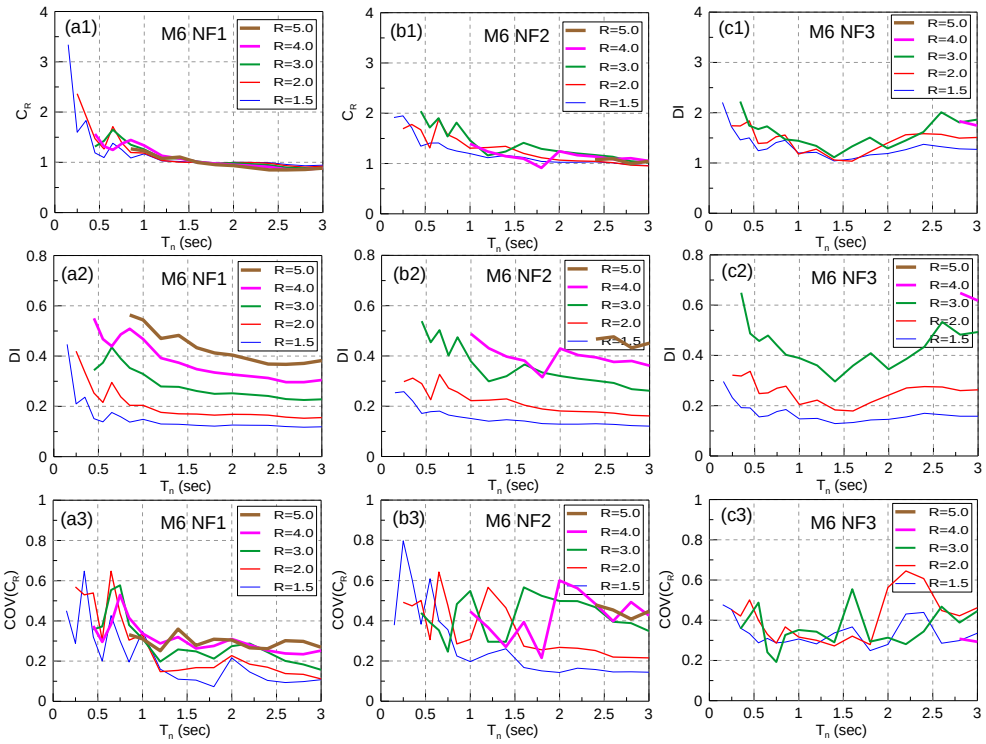

Fig. 4 – Mean C_R and corresponding DI spectra for M6 (SHM) model under: (a) NF1; (b) NF2; (c) NF3

Regarding the effects of column design parameters on the calculated C_R and DI spectra, it can be concluded that for far-field ground motions, C_R is approximately independent of column design parameters while DI correlates positively (i.e., DI increases with increasing amount of some design parameter) with longitudinal reinforcement and axial load ratios, but negatively (i.e., DI decreases with increasing amount of some design parameter) with transverse reinforcement and aspect ratios. For near-fault ground motions, C_R is approximately independent of column design parameters for NF1, while slightly affected by some of the column design parameters for NF2 and NF3. The C_R correlates positively with aspect ratios, positively with longitudinal reinforcement ratios when $R \leq 2.0$, and negatively with longitudinal reinforcement ratios when $R \geq 3.0$. On the other hand, the DI of near-fault ground motions with respect to the column design parameters follows similar trend to that of far-field ground motions.

5. Proposed C_R and DI formulae

Considering the C_R formula of FHWA (2006) can satisfactorily predict the calculated C_R spectrum for far-field ground motions recorded on site class C (FFC), the proposed C_R and DI formulae were constructed based on its functional form and were extended for the other cases. Figure 5 illustrates the proposed methodology used to determine the period limits in different design scenarios, where the period of vibrations corresponding to DI = 1.0 on the DI spectrum indicate the period limits that are applicable on the C_R spectrum. Also plotted in the figures are some of the calculated spectra for comparison. Notwithstanding this method would result in overestimation of DI in the vicinity of the period limit where there is only 20% probability of failure, it is thought to be expedient considering that approaching the period limit is normally prone to damage. By using

nonlinear regression analysis of the calculated results, the proposed C_R and DI formulae for far-field ground motions are given as follows.

$$C_R = \begin{cases} \left(1 - \frac{1}{R}\right)\frac{T_1^*}{T_n} + \frac{1}{R} \geq C_{R\_min}, & T_n \leq T_1^* \\ C_{R\_min}, & T_1^* < T_n \leq 3.0s \end{cases} \quad (6a)$$

$$T_1^* = \begin{cases} 1.25T_s & (Site\ Class\ C) \\ 1.45T_s & (Site\ Class\ D) \end{cases} \quad (6b)$$

$$C_{R\_min} = \begin{cases} 1.0 & (Site\ Class\ C) \\ 1.1 & (Site\ Class\ D) \end{cases} \quad (6c)$$

$$DI = \begin{cases} \left(C_{DI} - \frac{C_{DI}}{R}\right)\left(\frac{T_2^*}{T_n}\right)^n + \frac{C_{DI}}{R}, & T_n \leq T_2^* \\ C_{DI}, & T_2^* < T_n \leq 3.0s \end{cases} \quad (7a)$$

$$T_2^* = \{0.37\ ln(R) + 1.3\}T_s \quad (7b)$$

$$C_{DI} = \begin{cases} \{0.065 - 0.010\ ln(AD) + 0.017LR - 0.013\ ln(TR)\}R & (Site\ Class\ C) \\ \{0.077 - 0.006\ ln(AD) + 0.015LR - 0.017\ ln(TR)\}R & (Site\ Class\ D) \end{cases} \quad (7c)$$

$$n = 0.1R + 1.1 \quad (7d)$$

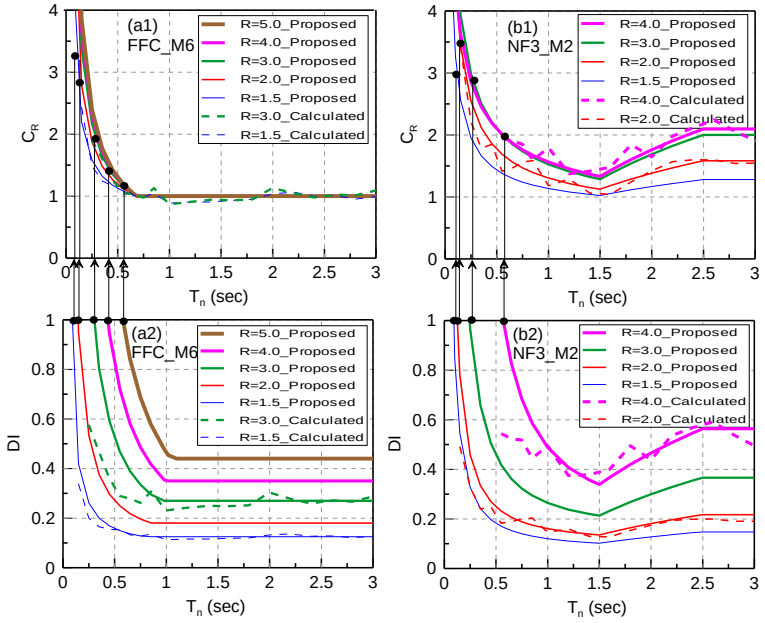

Fig. 5 – Illustration of proposed C_R and DI spectra for: (a) FFC; (b) NF3

It can be seen that the proposed C_R formula for FFC is exactly identical to that of FHWA (2006) but that for site class D (FFD) with minor modifications. In order to reflect the site effect on the computed spectra under FFD, the coefficient used to define the long period region is magnified to be 1.45, while a minimum C_R of 1.1 is imposed instead of the equal-displacement rule. On the other hand, the proposed DI formulae for the two site classes are correlated with the design parameters of column (Eq. 7c), where AD is the aspect ratio of column, LR is the percentile value of longitudinal reinforcement ratio, and TR is the ratio of transverse reinforcement to that required by the Caltrans bridge seismic design code (Caltrans 2003). The reason to normalize the transverse reinforcement by the code requirement is to allow for different amounts of reinforcing steels needed by circular and rectangular column sections to achieve comparable seismic behaviors. It should be noted that the computed spectra for M8 and M9 models were excluded from the regression analysis since their inclusion would cause unfavorable regression results. This may be attributed to their insufficient transverse reinforcements (around 75% of the code requirement) and the effect of applied axial load on the

amount of required transverse reinforcement, which needs further experimental and analytical efforts. Therefore, the proposed formulae are only applicable within the calibrated column design parameters, namely AD = 3 - 10, LR = 0.75 - 3.0, TR = 1.0 - 1.67, and axial load equal to around $0.1f_c'A_g$. For near-fault ground motions, the proposed formulae are given in Eqs. (8) and (9). To simplify the C_R formulae for near-fault ground motions, it was proposed not to correlate the formulae with the column design parameters even though there was minor correlation between them. Besides, the C_R and DI formulae for NF3 (T_p = 5.5 - 10.5 s) were divided into three segments where the increased spectral ordinate in long period region (T_n > 1.5 s) was expressed by a natural logarithm term associated with a constant term when T_n > 2.5 s.

$$C_R = \begin{cases} \left(C_{BR} - \frac{C_{BR}}{R}\right)\left(\frac{T_1^*}{T_n}\right)^{n_1} + \frac{C_{BR}}{R} + \frac{\Delta_1}{3}T_n, & T_n \le 3.0s\ (T_p = 0.5 \sim 5.5s) \\ \left(C_{BR} - \frac{C_{BR}}{R}\right)\left(\frac{T_1^*}{T_n}\right)^{n_1} + \frac{C_{BR}}{R}, & T_n \le 1.5s\ (T_p = 5.5 \sim 10.5s) \\ \left(C_{BR} - \frac{C_{BR}}{R}\right)\left(\frac{T_1^*}{1.5}\right)^{n_1} + \frac{C_{BR}}{R} + k_1 \times ln\left(\frac{T_n}{1.5}\right), & 1.5s < T_n \le 2.5s\ (T_p = 5.5 \sim 10.5s) \\ \left(C_{BR} - \frac{C_{BR}}{R}\right)\left(\frac{T_1^*}{1.5}\right)^{n_1} + \frac{C_{BR}}{R} + k_1 \times ln\left(\frac{2.5}{1.5}\right), & 2.5s < T_n \le 3.0s\ (T_p = 5.5 \sim 10.5s) \end{cases} \quad (8a)$$

$$T_1^* = 0.138R + 0.915 \quad (8b)$$

$$C_{BR} = \begin{cases} 1 & (T_p = 0.5 \sim 2.5s) \\ -0.069R^2 + 0.473R + 0.546 & (T_p = 2.5 \sim 10.5s) \end{cases} \quad (8c)$$

$$n_1 = \begin{cases} -0.106R + 1.149 & (T_p = 0.5 \sim 2.5s) \\ -0.113R + 0.967 & (T_p = 2.5 \sim 10.5s) \end{cases} \quad (8d)$$

$$\Delta_1 = \begin{cases} -0.02R + 0.22 & (T_p = 0.5 \sim 2.5s) \\ 0.1 & (T_p = 2.5 \sim 5.5s) \end{cases} \quad (8e)$$

$$k_1 = -0.2R^2 + 1.5R - 1.3 \quad (8f)$$

$$DI = \begin{cases} \left(C_{DI} - \frac{C_{DI}}{R}\right)\left(\frac{T_2^*}{T_n}\right)^{n_2} + \frac{C_{DI}}{R} + \frac{\Delta_2}{3}T_n, & T_n \le 3.0s\ \left(T_p = 0.5 \sim 2.5s\right) \\ \left(C_{DI} - \frac{C_{DI}}{1.5}\right)\left(\frac{T_2^*}{T_n}\right)^{n_2} + \frac{C_{DI}}{1.5} + \frac{\Delta_2}{3}T_n, & T_n \le 3.0s\ \left(T_p = 2.5 \sim 5.5s\right) \\ \left(C_{DI} - \frac{C_{DI}}{1.5}\right)\left(\frac{T_2^*}{T_n}\right)^{n_2} + \frac{C_{DI}}{1.5}, & T_n \le 1.5s\ (T_p = 5.5 \sim 10.5s) \\ \left(C_{DI} - \frac{C_{DI}}{1.5}\right)\left(\frac{T_2^*}{1.5}\right)^{n_2} + \frac{C_{DI}}{1.5} + k_2 \times ln\left(\frac{T_n}{1.5}\right), & 1.5s < T_n \le 2.5s\ (T_p = 5.5 \sim 10.5s) \\ \left(C_{DI} - \frac{C_{DI}}{1.5}\right)\left(\frac{T_2^*}{1.5}\right)^{n_2} + \frac{C_{DI}}{1.5} + k_2 \times ln\left(\frac{2.5}{1.5}\right), & 2.5s < T_n \le 3.0s\ (T_p = 5.5 \sim 10.5s) \end{cases} \quad (9a)$$

$$T_2^* = \begin{cases} 0.138R + 0.915 & (T_p = 0.5 \sim 2.5s) \\ C_1R^2 + C_2R + C_3 & (T_p = 2.5 \sim 10.5s) \end{cases} \quad (9b)$$

$$C_{DI} = \begin{cases} \{0.056 - 0.010\,ln(AD) + 0.028LR - 0.029\,ln(TR)\}R & (T_p = 0.5 \sim 2.5s) \\ \{0.075 - 0.009\,ln(AD) + 0.021LR - 0.027\,ln(TR)\}R & (T_p = 2.5 \sim 10.5s) \end{cases} \quad (9c)$$

$$n_2 = \begin{cases} -0.071R + 1.354 & (T_p = 0.5 \sim 2.5s) \\ C_1R^2 + C_2R + C_3 & (T_p = 2.5 \sim 10.5s) \end{cases} \quad (9d)$$

$$\Delta_2 = \begin{cases} 0.021R - 0.020 & (T_p = 0.5 \sim 2.5s) \\ 0.012 & (T_p = 2.5 \sim 5.5s) \end{cases} \quad (9e)$$

$$k_2 = 0.14R - 0.12 \quad (9f)$$

$$C_1 = 0.097 - 0.030\,ln(AD) + 0.060LR - 0.029\,ln(TR) \quad (9g)$$

$$C_2 = -0.340 + 0.083\,ln(AD) - 0.163LR + 0.092\,ln(TR) \quad (9h)$$

$$C_3 = 1.490 - 0.060\,ln(AD) + 0.142LR - 0.102\,ln(TR) \quad (9i)$$

5. Application to performance-based seismic design

The proposed capacity-based inelastic displacement spectra could be applied to the performance-based seismic design of reinforced concrete bridges. Different from the current trend of seismic design codes whose performance objective was based upon displacement or displacement ductility, this research proposed to use the damage index (or damage state) as the performance objective for bridge design. Fig. 6 shows the flowchart of the proposed seismic design procedure.

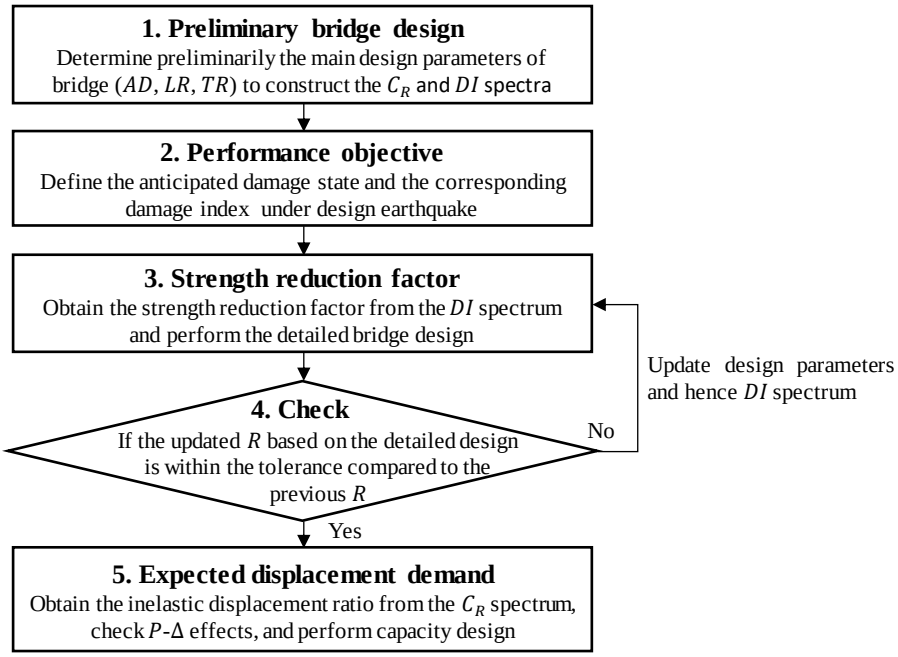

Fig. 6 – Flowchart of using capacity-based spectra in performance-based seismic design

6. Demonstrative example – seismic evaluation of three-span continuous concrete box girder bridge

To demonstrate the applicability of the proposed capacity-based inelastic spectra to seismic evaluation of RC bridges, an example bridge is constructed and analyzed by using various structural analysis programs, such as SAP2000, OpenSees, and the smooth hysteresis model proposed by the authors. Nonlinear time history analyses are conducted for far-field (FFC) and near-fault (NF3) ground motions, and comparisons of the analytical results between different models are made.

6.1 Bridge data

The three-span prestressed reinforced concrete box girder bridge shown in Fig. 7 will be used as demonstrative example bridge. The bridge has identical span length of 45 m and identical column height of 8.2 m. The columns are fixed at the bottom where the soil-structure interaction is not considered. On the other hand, the bridge deck is supported by two hinge bearings at each of the middle two bents, and by two roller bearings at each of the end bents along the longitudinal direction of bridge. However, in the transverse direction of bridge, the roller bearings at the end bents are locked to prevent lateral movement. The example bridge is assumed to be located in Nantou county of central Taiwan, which is near the Chelungpu fault. The soil condition at bridge site is Type D. The peak ground acceleration for design and maximum credible earthquakes at bridge site is around 0.36g and 0.45g, respectively. Based on the design spectrum for maximum credible earthquake (MOTC, 2009), the bridge columns are proportioned to have force reduction factors of around 2.9 and 1.5 in the longitudinal and transverse directions of bridge, respectively. The column reinforcement details can be found in Fig. 7.

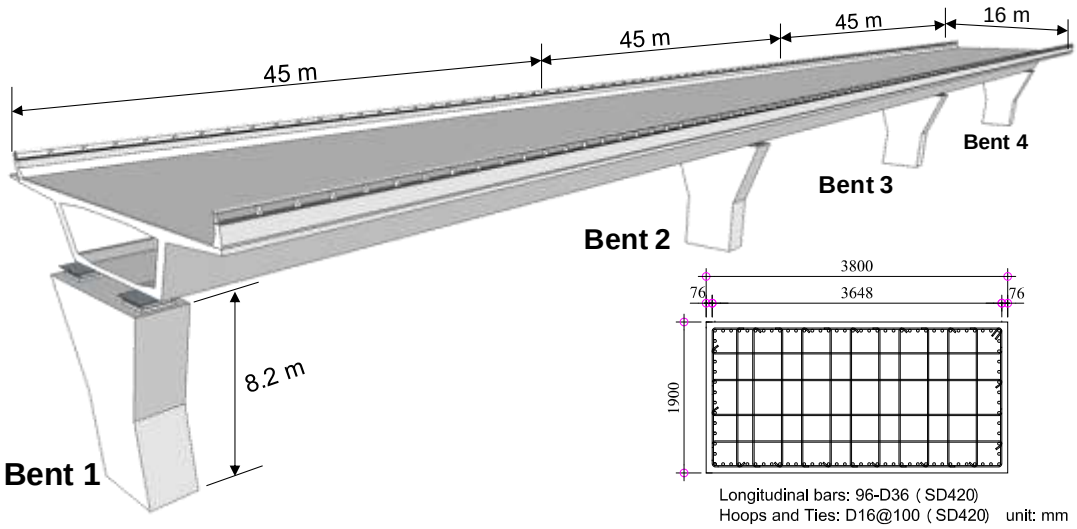

Fig. 7 – Example bridge

6.2 Seismic evaluation of example bridge

The bridge model is constructed in SAP2000 and OpenSees softwares. The fundamental period of vibrations are 0.82s and 0.46s for longitudinal and transverse vibration modes, respectively. In the SAP model, the nonlinear link element is placed at the bottom of bridge column to simulate the hysteresis behavior of RC column, where the Takeda hysteresis model are used (but actually, it should be the modified Clough model since the unloading stiffness does not degrade under hysteresis). In the OpenSees model, the force-based beam-column element with fiber section is used to simulate the nonlinear behavior of bridge columns. Besides, a SDOF system that uses the proposed smooth hysteresis model is also constructed to simulate the example bridge, considering that the seismic behavior of the bridge is mainly dominated by its fundamental mode (i.e., the corresponding modal mass participation factor is larger than 90%).

Table 2 – Comparisons of analytical results between three models

NF3	SHM			OPN			SAP		
No.	Δ_{max}(mm)	Δ_{min}(mm)	Δ_i(mm)	Δ_{max}(mm)	Δ_{min}(mm)	Δ_i(mm)	Δ_{max}(mm)	Δ_{min}(mm)	Δ_i(mm)
NF301	154.8	-208.2	208.2	124.2	-178.4	178.4	54.2	-200.5	200.5
NF302	234.4	-107.4	234.4	215.2	-94.7	215.2	222.7	-90.8	222.7
NF303	87.5	-183.8	183.8	91.4	-170.9	170.9	74.6	-156.9	156.9
NF304	337.1	-138.0	337.1	209.9	-115.1	209.9	199.2	-95.3	199.2
NF305	151.9	-167.6	167.6	122.0	-166.0	166.0	128.6	-196.8	196.8
NF306	114.9	-126.2	126.2	84.9	-189.2	189.2	93.4	-176.8	176.8
NF307	150.3	-242.3	242.3	123.0	-221.0	221.0	146.4	-172.3	172.3
NF308	289.9	-217.2	289.9	265.4	-193.7	265.4	265.9	-161.7	265.9
NF309	132.1	-169.3	169.3	122.7	-139.4	139.4	128.3	-120.5	128.3
NF310	223.5	-244.6	244.6	195.9	-213.8	213.8	228.4	-163.4	228.4
NF311	160.9	-155.0	160.9	135.4	-134.2	135.4	133.8	-102.4	133.8
NF312	451.9	-301.6	451.9	382.5	-234.3	382.5	321.8	-237.2	321.8
NF313	116.2	-275.0	275.0	110.5	-221.9	221.9	114.8	-233.6	233.6
NF314	Collapse	Collapse	Collapse	449.7	-597.6	597.6	530.6	-528.8	530.6
NF315	Collapse	Collapse	Collapse	634.8	-573.2	634.8	661.2	-572.4	661.2
AVG=	**200.4**	**-195.1**	**237.8**	**167.9**	**-174.8**	**208.4**	**162.5**	**-162.1**	**202.8**
Error(%)=	**0.0**	**0.0**	**0.0**	**-19.3**	**-11.6**	**-14.1**	**-23.4**	**-20.3**	**-17.2**

Nonlinear time history analyses are conducted in the longitudinal direction of bridge using the three models when subjected to 15 FFC and 15 NF3 ground motions. The ground motion records are normalized to have force reduction factors of 5 and 3 at the fundamental period of bridge for FFC and NF3, respectively.

Table 2 lists the computed maximum displacements of the three bridge models under NF3. Also shown in the end of the table are the average results of the 15 ground motions. It can be found that both the SAP and OpenSees models would lead to underestimation of maximum inelastic displacement when compared to the proposed smooth hysteresis model. Based on the assumption that the proposed smooth model can realistically reproduce the seismic response of the bridge, the SAP and OpenSees models could underestimate the maximum inelastic displacements by around 20% and 15%, respectively, under NF3. On the other hand, the underestimations of the two models would reduce to 12% and 7% under FFC. Therefore, it is suggested that the analytical displacements from the SAP and OpenSees models be appropriately magnified to avoid unconservative evaluation results. Besides, it is demonstrated by the example bridge that the proposed spectral formula can predict well the inelastic displacement and the corresponding damage index of the bridge when compared to those by the proposed smooth hysteresis model.

7. Conclusions

Capacity-based inelastic displacement spectra that comprise an inelastic displacement ratio (C_R) spectrum and the corresponding damage index (DI) spectrum are proposed in this study. It is demonstrated that the Park and Ang's damage index can be a good indicator for assessing the actual visible damage condition of column regardless of its loading history, providing a better insight into the seismic performance of bridges. The computed spectra show that the inelastic response of a structural system increases as the pulse period of a near-fault ground motion increases. Moreover, for R = 5.0, nearly all of the practical design scenarios of bridge considered in this research could not survive the near-fault ground motions with T_p= 5.5s - 10.5s. Finally, it is demonstrated by an example bridge that the proposed spectral formula can predict well the inelastic displacement and the corresponding damage index of the bridge, and both the SAP and OpenSees models could underestimate the inelastic responses of the brdige.

8. References

[1] Vamvatsikos D, Cornell CA (2002): Incremental dynamic analysis. *Earthquake Engineering & Structural Dynamics*, **31** (3), 491-514.

[2] Gurvich MR, Clavette PL, Costiner S (2014): Probabilistic test/model integrated analysis of composite materials and structures. *14th Pan-American Congress of Applied Mechanics PACAM XIV*, Santiago, Chile.

[3] Federal Highway Administration, FHWA (2006): Seismic Retrofitting Manual for Highway Structures: Part 1-Bridges, FHWA-HRT-06-032, McLean, VA.

[4] American Association of State Highway and Transportation Officials, AASHTO (2011): Guide Specification for LRFD Seismic Bridge Design, LRFDSEIS-2, Washington, DC.

[5] California Department of Transportation, Caltrans (2013): Seismic Design Criteria (SDC), Version 1.7, Sacramento, CA.

[6] Federal Emergency Management Agency, FEMA (1997): NEHRP Guidelines for the Seismic Rehabilitation of Buildings. Report FEMA 273, Washington, DC.

[7] Wang PH, Ou YC, Chang KC. (2017): A new smooth hysteretic model for ductile flexural-dominated reinforced concrete bridge columns. Earthquake Engineering and Structural Dynamics; 46:2237-2259.

[8] Park YJ, Ang AHS (1985): Mechanistic seismic damage model for reinforced concrete. Journal of Structural Engineering (ASCE); 111(4):722–739.

[9] Wen YK (1976): Method for random vibration of hysteretic systems. Journal of the Engineering Mechanics Division (ASCE); 102:249-263.

[10] Wang PH, Chang KC. Ou YC (2019): Capacity-based inelastic displacement spectra for reinforced concrete bridge columns. Earthquake Engineering and Structural Dynamics. (published online)

[11] MOTC (2009): Seismic bridge design specifications, Ministry of Transportation and Communications (MOTC), Taiwan. (in Chinese)